Spectral properties of classical two-dimensional clusters

Vitaly A. Schweigert* and François M. Peeters†
Departement Natuurkunde, Universiteit Antwerpen (UIA), Universiteitsplein 1, B-2610 Antwerpen, Belgium
(Received 16 September 1994)

We present a study of the spectral properties such as the energy spectrum, the eigenmodes, and the density of states of a classical finite system of two-dimensional charged particles which are confined by a quadratic potential. Using the method of Newton optimization we obtain the ground state and the metastable states. For a given configuration the eigenvectors and eigenfrequencies for the normal modes are obtained using the Householder diagonalization technique for the dynamical matrix whose elements are the second derivative of the potential energy. For small clusters the lowest excitation corresponds to an intershell rotation. The energy barrier for such rotations is calculated. For large clusters the lowest excitation consists of a vortex/antivortex pair. The Lindeman melting criterion is used to calculate the order-disorder transition temperature for intershell rotation and intershell diffusion. The value of the transition temperature at which intershell rotation becomes possible depends very much on the configuration of the cluster, i.e., the distribution of the particles between the different shells. Magic numbers are associated with clusters which are most stable against intershell rotation. The specific heat of the cluster is also calculated using the Monte Carlo technique, which we compare with an analytical calculation where effects due to anharmonicity are incorporated.

I. INTRODUCTION

During the past few years considerable attention has been paid to the study of the properties of systems consisting of a finite number of neutral or charged particles. The particles are confined by an artificial external confining field. Behavior of either ions in a radio-frequency trap (Paul trap) or a Penning trap[1,2] and heavy-ion ring storage[3] can serve as an illustration of three-dimensional (3D) Coulomb clusters. Very large Coulomb clusters have been created recently in strongly coupled rf dusty plasmas.[4] Examples of two-dimensional (2D) Coulomb clusters are electrons on the surface of liquid He (Ref. 5) and electrons in quantum dots.[6] The vortex clusters in an isotropic superfluid[7] and in superconducting grains[8] have many common features with those of 2D charged particles.[9] References 10, 11 have been devoted to the investigation of the ground state of 3D clusters of charged particles. Below we give a short overview of previous theoretical work on 2D clusters of charged particles.

Clusters of particles in 2D with Coulomb repulsion were investigated by Lozovik and coworkers,[12] in the case of parabolic confinement. They found that for low temperature and in the case of a small number of particles, the cluster has a shell structure. A two-step order-disorder transition was found. With increasing temperature, first intershell rotation starts, and intershell diffusion may be possible at high temperature. When the size of the cluster is sufficiently large, the simple shell structure gradually disappears in the center and features of a Wigner lattice appear. Then cluster melting occurs around the 2D Wigner lattice melting temperature.

Bolton and Rössler[13] considered the case of parabolic confinement for a small number of particles: 1–40. They investigated the ground state as well as some metastable states. For clusters consisting of six particles they determined the barrier height for transition from the configuration (1,5) (these are the number of electrons in each shell) to the configuration (6).

Systematic and detailed investigation of the structure of 2D clusters was carried out by Bedanov and Peeters.[14] They considered both parabolic and hard-wall confinement. A table of Mendeleev was constructed for clusters with 2–52, 82, 151, 230 number of particles. Using the Lindeman melting criterion these authors determined the temperature for the order-disorder transition for angular and radial displacement.

In all of the above works on 2D systems with a finite number of charged particles, the Monte Carlo simulation technique was used. We found that in some cases this method is rather slow in finding the ground state of the cluster. The reason is that the Monte Carlo technique spends too much time in the vicinity of metastable states such that for a finite simulation time the correct ground state is not necessarily found. This becomes more of a problem for clusters with larger number of particles, which have many more metastable states. In Ref. 14, this drawback was partially avoided by heating up the system and cooling it down repeatedly. In the present work, we will present an alternative approach. To find the ground state, we choose the Newton method with initial configurations determined randomly. In this way, we are able to obtain not only the ground state but also the metastable states. The latter are relevant in the calculation of thermodynamic properties and the barrier height for intershell rotation.

In previous work,[12–14] the ground-state properties and melting temperatures were obtained. Here, we will investigate the spectral properties of the system. This paper

is organized as follows. In Sec. II, we describe the model and introduce the dimensionless units. In Sec. III, our numerical technique to obtain the ground and metastable states is outlined and compared to the Monte Carlo technique. Section IV is devoted to the stable configurations and the spectrum of normal modes is determined. The barrier height for intershell rotation is obtained in Sec. V. Intershell rotation is the lowest excitation for small clusters. We correlate the strong dependence of the height of the barrier for intershell rotation to the number of particles placed in various shells. In Sec. VI, we discuss large clusters for which we calculate the density of states and discuss their lowest excitation which consists of a vortex/antivortex pair. In Sec. VII, the zero-temperature results for the excitation spectrum are used in order to calculate the melting temperatures using the Lindeman melting criterion. These results are compared with earlier results,[14] which were based on the Monte Carlo simulation technique. As an example of the use of metastable states in the calculation of thermodynamic property, we calculate the heat capacity in Sec. VIII. We compare the Monte Carlo results with an analytical approach in which we include anharmonicity effects in an approximate way. Our conclusions are presented in Sec. IX.

II. MODEL SYSTEM

The model system was defined in Ref. 14. But for completeness, we recall the main features. Our system is described by the Hamiltonian,

$$H = \frac{q^2}{\epsilon} \sum_{i>j} \frac{1}{\mid \vec{r}_i - \vec{r}_j \mid} + \sum_i V(\vec{r}_i), \tag{1}$$

where q is the particle charge, ϵ is the dielectric constant of the medium, the particles are moving in, and the confinement potential $V(\vec{r}) = \frac{1}{2} m\omega_0^2 r^2$ is taken parabolic. Particle motion is described by classical mechanics in the plane $\vec{r} = (x, y)$. To exhibit the scaling of the system, we introduce the characteristic scales in the problem: $r_0 = (2q^2/m\epsilon\omega_0^2)^{1/3}$ for the length, $E_0 = (m\omega_0^2 q^4/2\epsilon^2)^{1/3}$ for the energy, and $T_0 = (m\omega_0^2 q^4/2\epsilon^2)^{1/3} k_B^{-1}$ for the temperature. These scales will be used as our new units and all our results will be given in these units. In so doing, the Hamiltonian can be written as

$$H = \sum_{i>j} \frac{1}{\mid \vec{r}_i - \vec{r}_j \mid} + \sum_i V(\vec{r}_i), \tag{2}$$

with $V(\vec{r}) = x^2 + y^2$. The numerical values for the parameters ω_0, r_0, E_0, T_0 for some typical experimental systems were given in Ref. 14.

In the present paper, we will consider only classical systems. Although a classical approach for the description of the behavior of electrons in quantum dots is not applicable, nevertheless it is possible that certain features of the classical system may survive in a quantum system. For example, in the quantum study of the transition from a crystal to a liquid in the absence of a magnetic field,[15] we know that the parameter for formation of a Wigner crystal is $r_s = l_0/a_0 = 37 \pm 5$, where l_0 is the mean distance between the particles. If the number of particles is small, the interparticle distance in the case of parabolic confinement is close to r_0. Thus, for typical parameters for a quantum dot in GaAs with $m = 0.067$, $\epsilon = 13$, $\hbar\omega_0 = 1$ meV, we obtain $r_s = 7.8$. Reducing the confinement ω_0 or applying a magnetic field[16] will give us a possibility to investigate the existence of a Wigner crystal or another ordered state for a finite number of particles. In Ref. 14, it was found that a classical 2D cluster with a finite number of charged particles can be more or less stable than a 2D crystal, which has the same value for the parameter $\Gamma = q^2/\epsilon l_0 k_B T$. We expect that a similar quantity will be relevant in the quantum case and, therefore, it is expected that also a Wigner crystal like state can exist in quantum dots.

III. NUMERICAL APPROACH

The Monte Carlo simulation technique[17] is relatively simple and provides relatively rapid convergence and a reliable estimate of the total energy of the system in cases that a relative small number of Metropolis steps is sufficient. However, the accuracy of this method in calculating the explicit states may be poor in certain cases. We can understand this as follows: for the present system of axial symmetric confinement, some configurations have very small frequencies for intershell rotation $\omega_{\min} = 10^{-3}$–10^{-4}, which may lock the simulation in an unstable state. Using the Monte Carlo method with an acceptable number of steps 10^4–10^5, in order to limit the computer time, we may obtain the energy E up to an error δ. But the error in the coordinates will be proportional to $\delta^{1/2}/\omega_{\min}$, which in such a case can be large.

To circumvent this problem we used a different numerical approach, which is mainly based on our experience from which we learned that with different modifications to the gradient method and the method of molecular dynamics using artificial viscosity, we were able to obtain more reliable results than with the Monte Carlo technique. To be more explicit, to find the state with the minimal energy, we used the modified Newton technique. Since this method is practically not applied in the present field, we will give a short outline. Let us suppose that the coordinates of the particles in a cluster are given by $\{r^n_{\alpha,i};\ \alpha = x, y;\ i = 1, \ldots N\}$, after n steps in the simulation. Then the potential energy in the vicinity of this configuration can be written in the following quadratic form:

$$H = H(r^n_{\alpha,i}) - \sum_i \sum_\alpha H_{\alpha,i}(r_{\alpha,i} - r^n_{\alpha,i}) + \frac{1}{2} \sum_{i,j} \sum_{\alpha,\beta} H_{\alpha\beta,\,ij}(r_{\alpha,i} - r^n_{\alpha,i})(r_{\beta,j} - r^n_{\beta,j}), \tag{3}$$

where $H_{\alpha,i} = -\partial H/\partial r_{\alpha,i}$ is the force and $H_{\alpha\beta\,,ij}$ is the dynamical matrix,

$$H_{\alpha\beta,\,ij} = \frac{\partial^2 H}{\partial r_{\alpha,i} \partial r_{\beta,j}}. \tag{4}$$

The next step in our simulation is based on the condition of minimal total energy, which leads to

$$\sum_j \sum_\beta (\eta \delta_{\alpha\beta,ij} + H_{\alpha\beta,ij})(r_{\beta,j} - r^n_{\beta,j}) = H_{\alpha,i}, \quad (5)$$

where $\delta_{\alpha\beta,ij}$ is the unit matrix and the coefficient η is added to assure the stability of the algorithm. It is easy to show that the iteration procedure converges if $\eta > -\lambda_{\min}$, where $\lambda_{\min}$ is the minimal eigenvalue of the dynamical matrix. The system of linear equations (5) is solved using Gaussian elimination. The calculation of the matrix and solving the system of linear equations takes about N^2 numerical operations. This is equivalent to a Monte Carlo step, where also about N^2 operations are needed to find the energy, but the coefficient in front of N^2 is less for the latter. The reason is that to obtain the spectrum of the matrix is more laborious. The usual approach guarantees only convergence in the vicinity of the minimum. Therefore, we introduced an empirical dumping coefficient η. In the first few iterations, the value for η is set to be large: $\eta = 10$–100. If in the next step, the total energy of the system decreases the dumping coefficient is reduced, while in the opposite case, the value η is increased. From our experience, we know that such an algorithm for choosing the dumping parameter guarantees convergency of the iteration process. Furthermore, near the last steps, the dumping parameter becomes less than the minimal value of the eigenvalue of the dynamical matrix and the rate of convergency becomes square ($\delta_{n+1} \sim \delta_n^2$). The accuracy of the calculated energy δ is now only limited by rounding errors. For systems with axial symmetry there exists an eigenvalue with value zero, which corresponds to turning the system as a whole around the axis of symmetry. In such a case, the second eigenvalue λ_2 has to be taken as the minimal eigenvalue. We found that about 10–100 steps are needed in order to obtain an accuracy of 10^{-9}–10^{-10}. The exact number of steps depends on the number of particles.

After finding the state with the minimal energy, we calculate the eigenvalues and eigenvectors of the dynamical matrix (4). The eigenfrequencies of it are the eigenvalues squared. The condition that the minimal eigenvalue is positive guarantees that the obtained configuration is stable. Of course, also, the present method does not guarantee that all stable and metastable configurations, and the configuration with the lowest energy are found. To overcome this difficulty partially, we consider a large number (typically 200) of initial configurations which are generated randomly. From these initial configurations a few stable configurations remain, the number of which increases fast when $N > 30$–40. Among these stable configurations, the state with the lowest energy is taken to be the ground state of the system. The fact, that usually the state with the minimal energy is achieved already after a small number of steps, gives us confidence that this is likely the actual ground state of the cluster. Usually, the radius of convergence of the ground state is sufficiently large. We confirmed that the present approach for $N < 80$ leads to the ground-state configurations of Ref. 14, which were obtained using the Monte Carlo method with about 10^5–10^6 simulation steps.

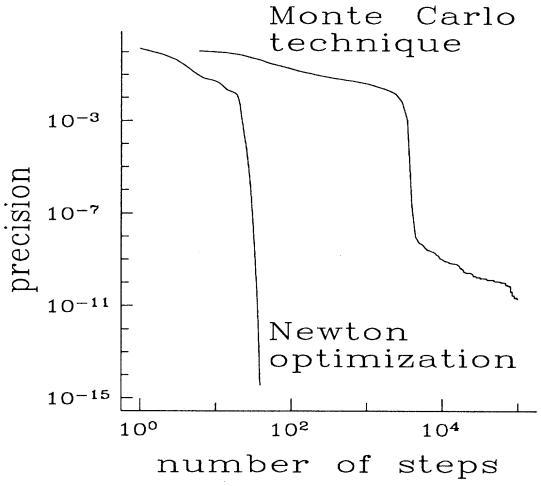

FIG. 1. Accuracy of the calculated ground-state energy versus the number of simulation steps, using the Monte Carlo technique, and the present optimized version of the Newton technique for a cluster consisting of $N = 13$ particles.

The efficiency of the present method is illustrated in Fig. 1. We plot the precision of the energy, which is defined as the difference from the exact energy value, as a function of the number of simulation steps for a cluster of 13 particles. It is apparent that the present technique converges much faster, an increase with a factor of about 200 is found. Furthermore, we discovered that for $N = 13$, even if within the Monte Carlo approach the error in the energy is only of order 10^{-11}, the obtained cluster configuration was unstable. This conclusion was reached by calculating the minimal eigenvalue of the dynamical matrix. For the case of Fig. 1, the configuration obtained with the Monte Carlo technique had a minimal eigenvalue, which was negative and, consequently, the configuration is unstable. The present Newton optimization approach did not exhibit such a deficiency. In contrast to the Monte Carlo approach used by Bolton and Rössler[13] who found more than one stable configuration for the case of $N = 13$ particles, the present approach in which 200 initial configurations were considered, demonstrates that there exist only one stable configuration, which is (4,9). But for this configuration the minimal excitation frequency $\omega_{\min} \approx 6 \times 10^{-4}$ is very small which may be the reason for the error in Ref. 13.

IV. EIGENVALUES AND EIGENVECTORS

A detailed description of the features of the lattice structure, the interparticle distance scale in the various shells, and the Mendeleev table for the configurations with $N = 2$–52, 82, 151, 230 particles was given in Ref. 14. Here, we will discuss the excitation spectrum corresponding to the ground-state configuration of the system. This spectrum is shown in Fig. 2, as function of the number of particles for even N ranging from 2 to 50. The eigenfrequency in this figure is in units of $\omega_0/\sqrt{2}$. Notice that there are three eigenfrequencies

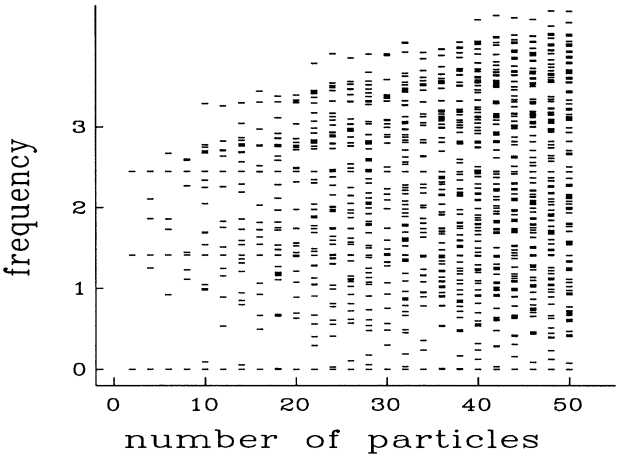

FIG. 2. Excitation spectrum of normal modes as a function of the number of particles in the cluster. The frequency is in units of $\omega_0/2^{1/2}$.

which are independent of N: (i) for any axial symmetric system the system as a whole can rotate, which gives an eigenfrequency $\omega = 0$. This is illustrated in Fig. 3 (figure indicated by $k = 1$; k counts the eigenvalues in increasing order) for a cluster of $N = 9$. The arrows indicate the direction of movement of the different particles (i.e., the eigenvectors of the excitation); (ii) there is a twofold degenerate vibration of the center of mass with frequency $\omega = \sqrt{2} = 1.4142$ (see Fig. 3, $k = 7$); and (iii) the third eigenfrequency corresponds to a vibration of the mean square radius $N^{-1}\sum_i (x_i^2 + y_i^2)$ with frequency $\omega = \sqrt{6} = 2.4495$ (see Fig. 3, $k = 15$). The value of this breathing mode can easily be obtained analytically.

For clusters of sufficient large size (i.e., $N > 8$), a typical feature of its spectrum is the occurrence of a very

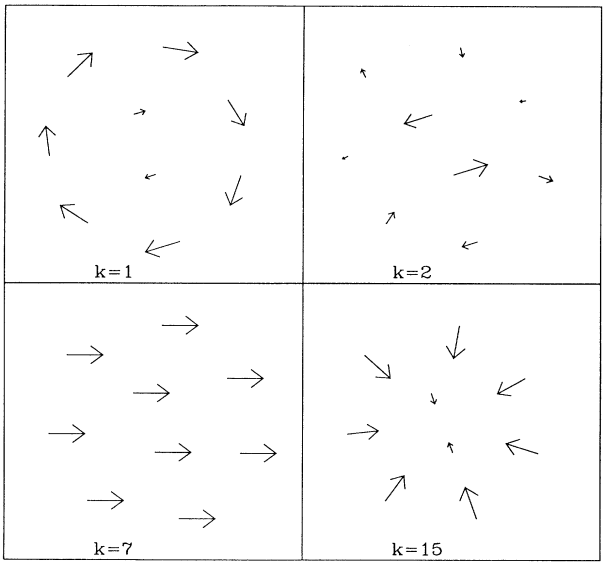

FIG. 3. Eigenvectors for a cluster with $N = 9$ particles for different mode number k, which corresponds to the eigenfrequencies $\omega_1 = 0$, $\omega_2 \approx 0.127$, $\omega_7 \approx 1.414$, $\omega_{15} \approx 2.449$.

low eigenfrequency. Because of the scale in Fig. 2, this frequency is not always discernable from the $\omega = 0$ frequency and, therefore, we have listed it in Table I as $\omega_{\min}$. For a number of clusters the eigenvectors corresponding to these minimal eigenvalues are shown in Figs. 3 ($k = 2$), 4, and 5 ($k = 2$). For $N = 19$ and $N = 20$, the central particle does not move for this specific excitation and, consequently, its displacement vector has length zero and is therefore not visible in Fig. 4. For the clusters with $N = 9$, 19, and 20 particles, the motion with the minimal frequency $\omega_{\min}$ corresponds to intershell rotation. The necessary condition for the existence of intershell rotation is the presence of at least two particles on the inner shell in order to conserve total angular momentum. With changing configuration, the minimal eigenfrequency can vary by several orders of magnitude (see Table I). For instance, for $N = 19$ with the ground-state configuration $(1, 6, 12)$, the minimal eigenfrequency is $\omega_{\min} \approx 0.67$, and for $N = 20$ and configuration $(1, 7, 12)$, $\omega_{\min} \approx 1.0 \times 10^{-4}$. In both cases the minimal eigenfrequencies correspond to intershell rotation (Fig. 4). This large change in the size of the minimal eigenfrequency is connected to the shell configuration, and not to the total number of particles. For example, if for $N = 19$ we take the metastable configuration $(1, 7, 11)$ whose energy is an amount 1.66×10^{-2} larger than the ground-state energy, we found numerically $\omega_{\min} \approx 1.1 \times 10^{-4}$, which coincides practically with $\omega_{\min}$ for the cluster with 20 particles.

From the data given in Table I, we infer the following law: *a high frequency value for intershell rotation is obtained for configurations such that the number of particles on the outer shell is an integral number times the number of particles on the inner shell.* For example, $N = 12$ $(3, 9)$, $N = 15$ $(5, 10)$, $N = 16$ $(1, 5, 10)$, and $N = 19$ $(1, 6, 12)$. For clusters with more than two shells (i.e., $N > 21$) a large $\omega_{\min}$ for intershell rotation is found for ground-state configurations, in which the number of particles in the different shells are multiples of an integer number. The latter is usually the number of particles in the inner shell. For example, $N = 22$ $(2, 8, 12)$, $N = 30$ $(5, 10, 15)$, $N = 45$ $(3, 9, 15, 18)$ and to a lesser extent also $N = 34$ $(1, 6, 12, 15)$. These cluster numbers can be considered as the *magic numbers*, because they represent the clusters which are most stable against intershell rotations. In previous work by others on 3D clusters, magic numbers were determined on the basis of energy calculations of the cluster configuration. We found[14] that for 2D clusters no clear steps are found in the cluster energy versus the number of particles in the cluster and, therefore, the stability argument is more appropriate in the present case. On the other hand, a configuration with small $\omega_{\min}$ for intershell rotation is realized when the number of particles in the different shells have no common divisor. For example, $N = 13$ $(4, 9)$ and $N = 20$ $(1, 7, 12)$.

The above rules can be understood from the Hamiltonian by analyzing the intershell interactions using cylindrical coordinates. Let us consider the most simple configuration with two shells. From the outset we notice that the occurrence of a particle in the center of the system, for example, for a cluster with 20 particles, does not dis-

turb the intershell rotation. Therefore, we do not have to consider such a case separately. Let us discuss the rotation between two outer shells. The interparticle distance and the distance between the shells changes only by a few percent when we alter the number of particles and/or the configuration. Therefore, in an initial approximation, we can describe each shell by an ideal polygon and, thus, the interaction Hamiltonian between two shells can be reduced to the form

$$H = \frac{1}{2}\sum_{i=1}^{N_1}\sum_{j=1}^{N_2}[R_1^2 + R_2^2 + 2R_1R_2\cos(i\theta_1 - j\theta_2 - \theta)]^{-1/2}, \quad (6)$$

where R_1, R_2, $\theta_1 = 2\pi/N_1$, $\theta_2 = 2\pi/N_2$ are the radii and angles between particles of the first and second shell, which have N_1 and N_2 particles, respectively, and θ is the

TABLE I. Shell configuration $(N_1, N_2, \ldots)$ for clusters with N particles with parabolic confinement. The minimal excitation frequency ($\omega_{\min}$ in units of $\omega_0/\sqrt{2}$), the period (φ_*) in degree units, and the barrier height (U_*) for intershell rotation are given together with the parameter R_* for the ground state of the cluster.

N	$N_1, N_2, \ldots$	$\omega_{\min}$	φ_*	U_*	R_*
9	2,7	1.268×10^{-1}	24.9	8.44×10^{-5}	1.349
10	2,8	8.910×10^{-2}	43.9	1.20×10^{-4}	1.427
11	3,8	2.451×10^{-2}	14.2	2.42×10^{-6}	0.882
12	3,9	5.308×10^{-1}	38.3	7.33×10^{-3}	0.912
13	4,9	6.002×10^{-4}	9.7	1.06×10^{-9}	0.672
14	4,10	4.940×10^{-2}	16.8	2.60×10^{-5}	0.644
15	5,10	4.599×10^{-1}	32.8	1.11×10^{-2}	0.564
16	1,5,10	4.924×10^{-1}	31.9	2.03×10^{-2}	0.449
17	1,6,10	5.416×10^{-2}	10.4	3.44×10^{-5}	0.374
18	1,6,11	6.141×10^{-3}	4.8	1.03×10^{-7}	0.360
19	1,6,12	6.676×10^{-1}	26.6	3.14×10^{-2}	0.396
20	1,7,12	1.031×10^{-4}	4.0	2.01×10^{-11}	0.334
21	1,7,13	3.174×10^{-3}	3.5	2.18×10^{-8}	0.294
22	2,8,12	2.934×10^{-1}	12.5	5.44×10^{-3}	0.257
23	2,8,13	1.287×10^{-1}	11.6	4.74×10^{-4}	0.258
24	3,8,13	2.762×10^{-2}	2.7	5.86×10^{-6}	0.118
25	3,9,13	1.138×10^{-1}	7.4	2.47×10^{-4}	0.210
26	3,9,14	1.041×10^{-1}	7.0	1.81×10^{-4}	0.212
27	4,9,14	1.311×10^{-2}	12.0	1.04×10^{-6}	0.611
28	4,10,14	5.682×10^{-2}	5.6	8.31×10^{-5}	0.179
29	4,10,15	3.911×10^{-2}	9.5	1.58×10^{-4}	0.183
30	5,10,15	2.974×10^{-1}	18.6	1.47×10^{-2}	0.172
31	5,11,15	2.351×10^{-2}	5.1	1.52×10^{-5}	0.167
32	1,5,11,15	2.971×10^{-2}	5.1	2.57×10^{-5}	0.137
33	1,6,11,15	6.805×10^{-2}	10.0	1.15×10^{-4}	0.257
34	1,6,12,15	2.379×10^{-1}	8.6	3.68×10^{-3}	0.131
35	1,6,12,16	6.585×10^{-2}	5.5	1.12×10^{-4}	0.134
36	1,6,12,17	8.963×10^{-3}	2.6	5.04×10^{-7}	0.131
37	1,7,12,17	3.214×10^{-3}	5.3	4.66×10^{-8}	0.317
38	1,7,13,17	6.134×10^{-3}	4.8	3.28×10^{-6}	0.113
39	2,8,12,17	2.231×10^{-1}			0.091
40	4,6,13,17	1.242×10^{-1}	14.8	2.21×10^{-3}	0.118
41	4,6,14,17	1.237×10^{-1}	4.8	5.90×10^{-4}	0.092
42	3,8,14,17	3.340×10^{-2}			0.096
43	3,9,14,17	5.010×10^{-2}	7.0	2.97×10^{-4}	0.200
44	3,9,14,18	1.552×10^{-1}	7.5	3.40×10^{-3}	0.092
45	3,9,15,18	1.962×10^{-1}	13.4	2.66×10^{-2}	0.094
46	3,9,15,19	8.425×10^{-1}	4.3	2.40×10^{-4}	0.093
47	4,10,15,18	1.850×10^{-1}			0.034
48	4,10,15,19	1.242×10^{-1}	9.1	2.37×10^{-3}	0.130
49	4,10,16,19	1.511×10^{-1}	6.2	2.05×10^{-3}	0.079
50	4,10,16,20	7.535×10^{-2}	12.0	3.32×10^{-3}	0.088
51	5,11,16,19	7.530×10^{-2}			0.189
60	1,7,13,18,21	7.420×10^{-2}	7.0	7.11×10^{-4}	0.059
70	6,6,15,20,23	1.220×10^{-2}			0.097
80	1,6,12,17,22,22	1.840×10^{-2}	4.9	1.19×10^{-5}	0.117

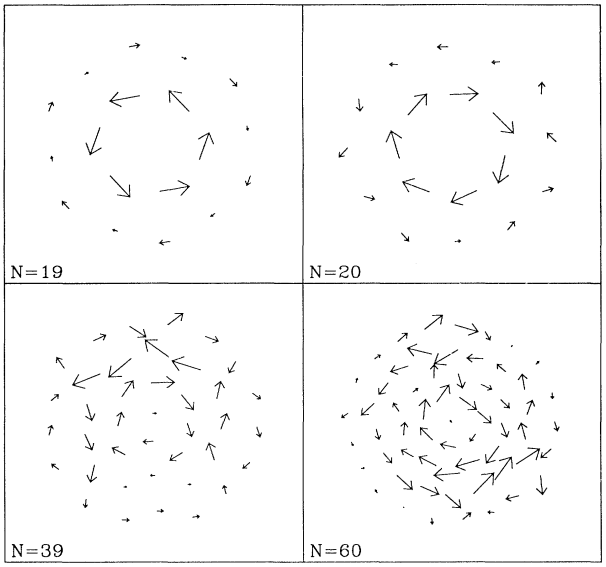

FIG. 4. Eigenvectors corresponding to the minimal frequency for clusters with $N = 19$, 20, 39, and 60 particles.

intershell angular distance. The sum (6) over the two indexes can be reduced to the sum over one index only,

$$H = \frac{N_1 N_2}{2I} \sum_{i=1}^{I} \left[R_1^2 + R_2^2 + 2R_1 R_2 \cos\left(i\theta_* - \theta\right)\right]^{-1/2}, \tag{7}$$

where

$$\theta_* = \frac{2\pi}{I}, \tag{8}$$

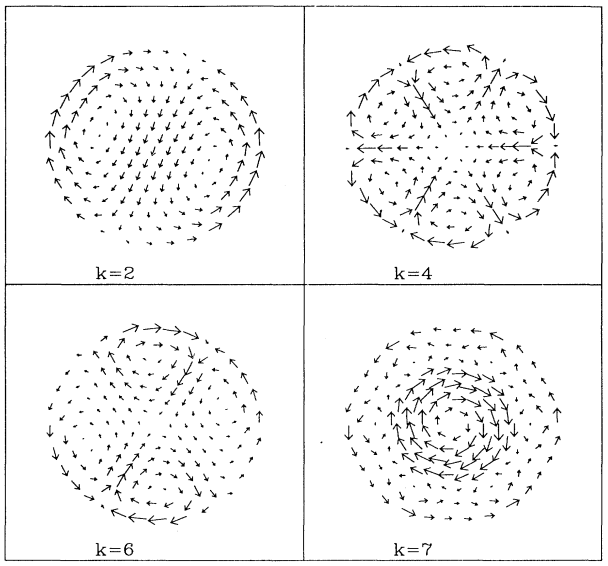

FIG. 5. Eigenvectors for the cluster with $N = 151$ particles for four different values of the mode number k.

and I is an integer, which is the minimal divisor of the number of particles (N_1, N_2, ...) in the different shells. From expression (7), it follows that the Hamiltonian for intershell interaction is periodic in θ. Moreover the period θ_*, as a rule, is less than the angular interparticle distance within a shell. To evaluate the strength of the intershell interaction energy, we deduct from the Hamiltonian the following value:

$$\frac{N_1 N_2}{4\pi} \int_0^{2\pi} dx \left[R_1^2 + R_2^2 + 2R_1 R_2 \cos\left(x - \theta\right)\right]^{-1/2}, \tag{9}$$

which is independent of θ. This result was obtained from Eq. (7) by replacing the summation over k by an integration. We proved that the error we make in doing so is proportional to θ_*^2. Numerical summation of (7) gives even a more weaker dependence of the interaction energy on N for two ideal polygons. When we compare the computed results for the barrier height for intershell rotation with those found from Eq. (9), we found that Eq. (9) gives a good qualitative description but quantitatively the results are not satisfactory. Therefore we may conclude that for small eigenvalues, the exact value of the barrier height is strongly influenced by the *nonideality* of the polygons. Indeed in order to obtain Eq. (6), we assumed that the particles were placed at the edges of an ideal polygon. Because intershell rotation is a collective phenomena, one can easily understand that the actual barrier height is less than that given by Eq. (7) due to the deformation of the polygons during the motion. Indeed, during the rotational motion not only the intershell distance changes but also the interparticle distance within a shell is altered. This is illustrated in Figs. 3 and 4. From these figures, we notice that the eigenvectors for the particles in the inner shell have practically the same length and are orthogonal to the radius vector of the particle. For the outer shell the situation is different and the eigenvectors have also components in the radial direction and futhermore, the length of the eigenvectors are different for the different particles (see Fig. 4). Therefore the vibrations in the radial and axial directions of the outer shell follow the intershell rotational motion of the particles. Only for clusters in which the number of particle on the inner shell is a multiplicative integer factor of those of the outer shell, i.e., when a large intershell rotation frequency is found, are the polygons almost ideal. This can be understood from symmetry reasons and from our numerical results. The characteristics and modeling of the intershell rotation will be given in next section.

When we increase the number of particles, we found that for $N = 39$ (see Fig. 4) the motion with the minimal eigenfrequency no longer corresponds to intershell rotation, but rather consists of rotation of different individual regions of the cluster. For $N \geq 60$ (see Fig. 4), the rotation of an innershell is followed by the rotation of individual polygons at the periphery of the cluster. For $N \geq 115$, we found that the minimal frequency $\omega_{\min}$ no longer corresponds to intershell rotation but corresponds to the excitation of a vortex/antivortex pair (see figure $k = 2$ of Fig. 5, which is for N=151). Higher excitations (see Fig. 5 with $k = 4$ and $k = 6$) may consist of

multiples of such pairs. In case of a cluster of $N = 151$ particles, the 7th lowest excitation corresponds now to an intershell rotation. A more detailed discussion on the nature of the low energy excitations of large clusters is postponed to Sec. VI.

V. BARRIER FOR INTERSHELL ROTATION

In the present section, we give a more detailed discussion of the lowest nontrivial excitation in case of small clusters: the intershell rotation. The barrier for intershell rotation was obtained using the following procedure. Let us assume that after n steps in our simulation the coordinates of the particles are given by $\{\vec{r}_i^n; i = 1, ..., N\}$. After diagonalizing the dynamical matrix $H_{\alpha\beta,ij}$, we obtain the eigenvectors $\vec{A}_i(k)$ and the eigenvalues $\lambda_k = \omega_k^2$. The time evolution of the particle coordinates is then given by

$$\vec{r}_i^{n+1} = \vec{r}_i^n + \sum_{k=2}^{2N} \tau_k \vec{A}_i(k) \ , \tag{10}$$

which determines also the next step in our simulation. The size of the time step is chosen by putting $\tau = \tau_{k^*}$ much smaller than the inverse of the frequency for intershell rotation, which is the lowest nonzero frequency in the spectrum. The values of all other coefficients τ_k are found from the condition of minimal potential energy. This is done as follows: substitute the above expression in Eq. (3), which gives us the total energy for the next step,

$$H_{n+1} = H_n + \sum_{i=1}^{N} \sum_{k=2}^{2N} \tau_k \frac{\partial H}{\partial \vec{r}_i} \cdot \vec{A}_i(k) + \frac{1}{2} \sum_{k=2}^{2N} \lambda_k \tau_k^2 \ , \tag{11}$$

from which we readily find the coefficients,

$$\tau_k = -\lambda_k^{-1} \sum_{i=1}^{N} \frac{\partial H}{\partial \vec{r}_i} \cdot \vec{A}_i(k) \ . \tag{12}$$

Trajectories of the particles for intershell rotation in four different clusters are depicted in Fig. 6. It is apparent that intershell rotation takes place in conjunction with radial oscillations. The latter are more noticeable for clusters with high symmetry (clusters $N = 9, 19$ in Fig. 6), which have a relative large frequency and, consequently, large barrier heights for intershell rotation. In clusters with only two shells, particles in different shells rotate in opposite direction in order to conserve total angular momentum. Such a motion is defined completely by the angle of rotation φ of one shell relative to the second. When there are three shells or more it is convenient to introduce the angle of rotation φ of the shell with the maximum angular velocity as an independent parameter. Figure 7 illustrates the dependence of the potential energy on this parameter φ for two different clusters with $N = 9$ and $N = 40$ particles. In general, this function is well approximated by the simple relation,

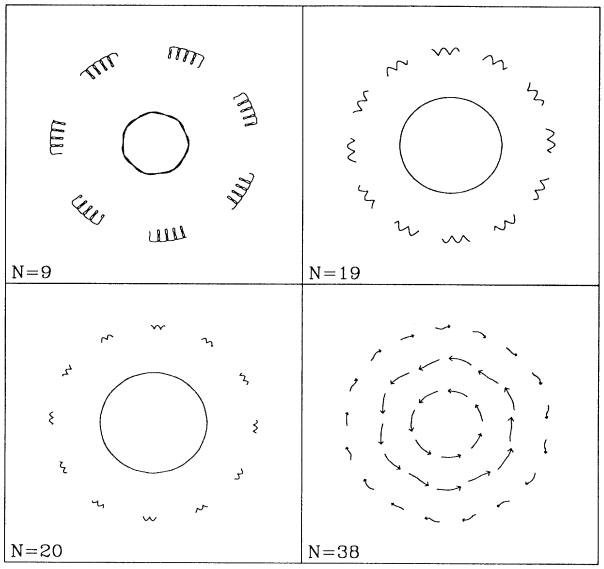

FIG. 6. Trajectories of the particles for intershell rotational motion in case of clusters of $N = 9$, 19, 20, and 38 particles.

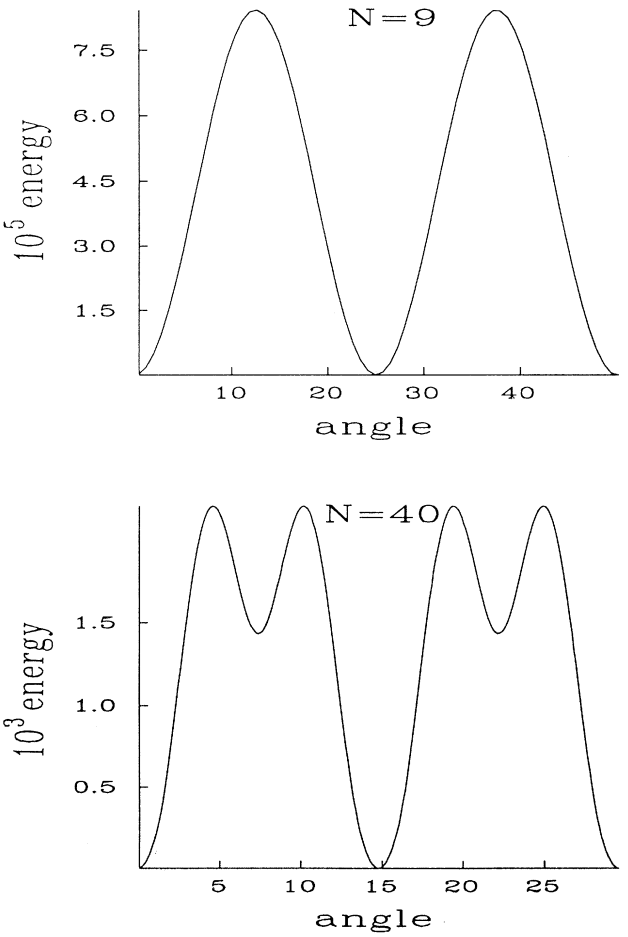

FIG. 7. Cluster energy versus shell turn angles (in degrees) for the shell with the maximal angular velocity for clusters with $N = 9$ and 40 particles.

$$U = \frac{U_*}{2}\left[1 - \cos\left(\frac{2\pi\varphi}{\varphi_*}\right)\right], \tag{13}$$

where U_*, and φ_* are the barrier height and the period, respectively. The values for U_* and φ_* are given in Table I. The above procedure is not able to give the value of the barrier height for the clusters $N = 39, 42, 47, 51$, and 70. The reason is that for those clusters the minimal eigenvalue does not correspond to intershell rotation. Notice that the cluster with $N = 40$ has two minima in the potential energy. One of this minima corresponds to a metastable state. Of course, U_* and φ_* in Table I are determined by the global minimum and maximum. In a few cases, the maxima in potential energy are sharper than that given by expression (13). The reason is that the energy for clusters with three and more shells are not only a function of the angular position of the shell.

For clusters with two shells, the parameter φ characterizes the motion of the inner shell. The angle of rotation of the outer shell relatively to the inner one can be obtained from the condition of zero total momentum,

$$\theta = \left(1 + \frac{N_1 R_1^2}{N_2 R_2^2}\right)\varphi\ , \tag{14}$$

where N_i, R_i are the number of particles and the radius of shell i, respectively. For clusters with two shells, the value φ_* presented in Table I is correctly approximated by taking the simple analytical formulas (8) and (14) equal to each other.

The Hamiltonian for intershell rotation, taking into account the angular kinetic energy, can be written in the form

$$H = \frac{1}{2}N_1 R_1^2 \dot{\varphi}^2 \left(1 + \frac{N_1 R_1^2}{N_2 R_2^2}\right) + \frac{1}{2}U_*\left[1 - \cos\left(\frac{2\pi\varphi}{\varphi_*}\right)\right]. \tag{15}$$

For clusters with more than two shells, we can only propose phenomenologic generalization to expression (15). Let us label $\{\vec{A}_i; i = 1, ..., N\}$ the set of eigenvectors corresponding to intershell rotation. Then to first approximation the Hamiltonian for intershell rotation becomes

$$H = \frac{1}{2}R_*^2\dot{\varphi}^2 + \frac{1}{2}U_*\left[1 - \cos\left(\frac{2\pi\varphi}{\varphi_*}\right)\right], \tag{16}$$

with

$$R_*^{-1} = \frac{1}{M}\sum_{i=1}^{M} |\vec{r_i} \times \vec{A}_i|/r_i^2\ , \tag{17}$$

where the summation is carried out over the particles of the shell, which has the maximum angular velocity. The value of the parameter R_* is also given in Table I. Once we have the Hamiltonian it is not difficult to find the connection between the barrier angular value φ_* and the characteristic frequency for intershell rotation,

$$U_* = 2\left(\omega_{\min}\frac{R_*\varphi_*}{2\pi}\right)^2 = 2(\omega_{\min}\delta)^2\ . \tag{18}$$

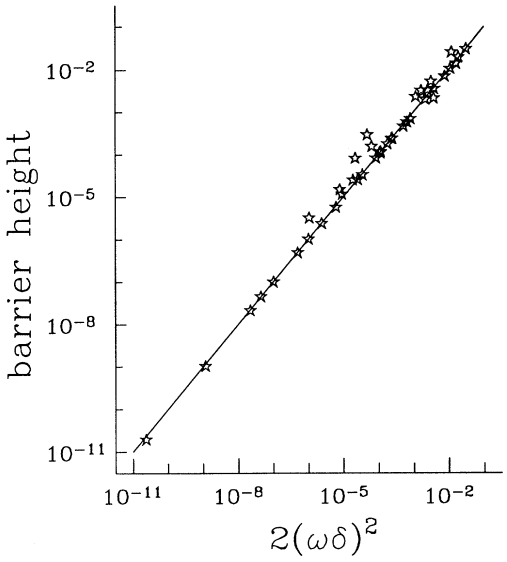

FIG. 8. Energy barrier of intershell rotation versus $(\omega\delta)^2$, where $\omega = \omega_{\min}$ is the frequency for intershell rotation and δ is the linear distance traveled by a particle over one angular period.

The parameter δ has a clear physical meaning: it is the length which a particle travels within a shell when it moves over the angle φ_*. The approximate expression (18) is shown in Fig. 8 by the solid curve together with the results of our simulation, which are given by the symbols. Notice that Eq. (18) describes our numerical results very well over an energy barrier height variation of more than eight orders of magnitude.

VI. DENSITY OF STATES AND VORTEX EXCITATIONS

From Fig. 2, we notice that the maximum frequency in the excitation spectrum, on the average, slowly increases with increasing number of particles. We can easily explain this with the aid of the theory of an infinite system. As it follows from our calculations, and has been mentioned in previous work,[14] the minimal interparticle distance decreases slowly with the growth of the cluster size due to the compression of the inner shell by particles placed at the periphery of the cluster. As a consequence, the maximum value of the wave vector $k \approx \pi/l_0$ (l_0 is the mean distance between the particles) and also the wave frequency will increase weakly with the cluster size.

For large clusters, it is more interesting to consider the density of states (DOS) of excitations (phonons), which can be obtained by a summation of the energy levels, displayed in Fig. 2, over a frequency interval which we took $\delta\omega = \omega_{\max}/40$, where $\omega_{\max}$ is the maximal eigenfrequency. The results for $N = 80$ and $N = 300$ particles is shown in Fig. 9. A characteristic feature in the DOS for all clusters is the occurrence of two broad maxima. From earlier investigations[18] of classical infinite 2D systems we know that there are two types of waves in a 2D Wigner

crystal: the lateral sound waves with dispersion relation $\omega \sim k$ and the longitudinal plasma wave with $\omega \sim \sqrt{k}$, in the long-wavelength limit. Using an analytical approximation for the frequency of sound $\omega_1^2 \approx 0.003\,63\omega_p^2 k^2 l_0^2$ and the plasma frequency $\omega_2^2 \approx \omega_p^2 k l_0(1 - 0.181\,483 k l_0)$, taken from Ref. 18, it is possible to show that the positions of the broad maxima in Fig. 9 are in qualitative agreement with the ones for an infinite crystal. In our dimensionless units, $\omega_p = 2\pi/\rho l_0$. To obtain the value of ω_p, we used the average particle density $\rho = N/\pi R_0^2$, where R_0 is the radius of the most outer shell. The maximum frequency of plasma like waves $\omega_{2,\max} \approx 1.17\omega_p$, for the cluster with $N = 80$ equals 4.67, and for $N = 300$ is about 5.77. Let us assume that the maximum frequency for sound waves is achieved at $kl_0 = \pi$. Then for $N = 80$ we obtain $\omega_{1,\max} \approx 2.38$ and for $N = 300$ we find $\omega_{1,\max} \approx 2.94$, which are slightly larger than the position of the first maximum appearing in Fig. 9.

From continuum elastic theory, a 2D electron crystal can be considered as incompressible at low frequencies.[19] In order to check if this is still the case for the present finite system, we consider the z component of the rotor $\Psi_r(k) = \vec{e}_z \cdot \mathrm{rot}\Psi(k)$ and the divergence $\Psi_d(k) = \mathrm{div}\Psi(k)$ of the field of eigenvectors of mode k,

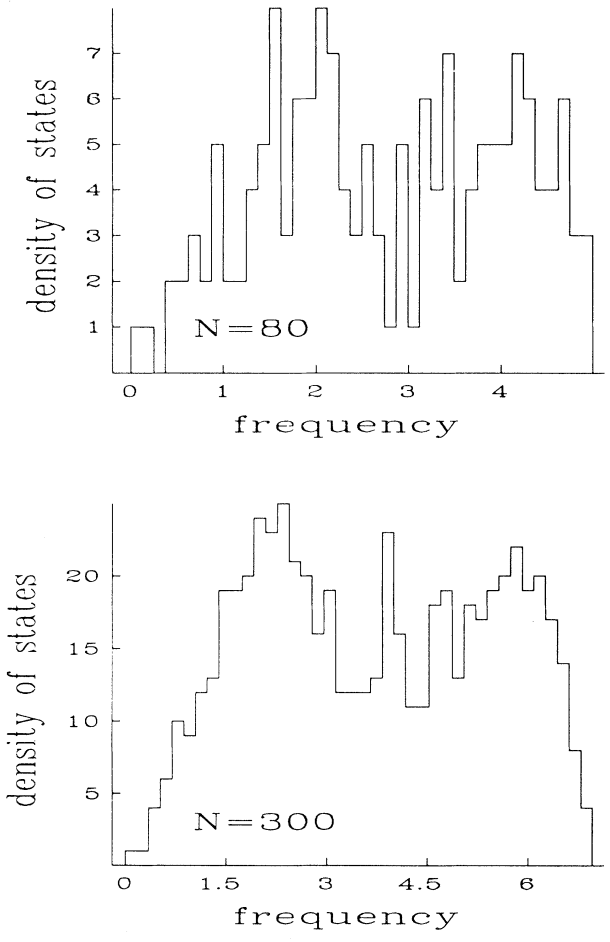

FIG. 9. Density of phonon states for clusters with $N = 80$ and 300 particles.

$$\Psi_d(k) = \frac{1}{N}\sum_{i=1}^{N} \psi_{d,i}^2(k), \tag{19a}$$

$$\Psi_r(k) = \frac{1}{N}\sum_{i=1}^{N} \psi_{r,i}^2(k)\ . \tag{19b}$$

The values $\psi_{d,i}(k)$, and $\psi_{r,i}(k)$ for the ith particle are given by

$$\psi_{d,i}(k) = (\vec{r}_i - \vec{r}_m) \cdot [\vec{A}_i(k) - \vec{A}_m(k)]/|\vec{r}_i - \vec{r}_m|^2\ , \tag{20a}$$

$$\psi_{r,i}(k) = |(\vec{r}_i - \vec{r}_m) \times [\vec{A}_i(k) - \vec{A}_m(k)]|/|\vec{r}_i - \vec{r}_m|^2\ , \tag{20b}$$

where $\vec{r}_m$ are the coordinates of the neighbor particles and $\vec{A}_i(k)$ is the eigenvector of particle i for mode k. The rotor and divergence of the eigenvector field are shown in Fig. 10 as a function of the excitation frequency for clusters of size $N = 80$ and $N = 300$. Notice that for small values of the frequency, the rotor of the field of eigenvectors is larger than the divergence. As a consequence, in a finite system but with N sufficiently large, the system is incompressible and one can expect that the low frequency excitation consists of vortex motion in which the particle density is not disturbed. From our computer calculations, we found that for $N = 151$ the minimum eigenfrequency corresponds indeed to the formation of a vortex/antivortex structure (Fig. 5). Since the total angular moment has to be equal to zero, those vortexes always come into pairs. With higher eigenvalues, the number of vortexes rises, although this function is not necessarily monotonic (see Fig. 5). Thus when N is sufficiently large, the cluster of charged particles can be described as a viscious noncompressible fluid in case of small wave vectors. Vortex motion is only expected for sufficiently large N, because the velocity of dissipation of the vortex energy is inversely proportional to R^2, where R is the characteristic radius, which increases with increasing N.

VII. MELTING TEMPERATURES

In Ref. 14, it was shown that the $T = 0$ ordered state of the cluster is destroyed with increasing temperature (T). The melting temperature for this order-disorder transition was obtained by investigating the radial displacement, the relative intrashell and intershell angular displacements as function of temperature. Here, we will start from the excitation spectrum of the zero-temperature ordered state in order to calculate the melting temperature using the Lindeman melting criterion.[20] In the harmonic approximation the mean square displacement is given by the following expression:

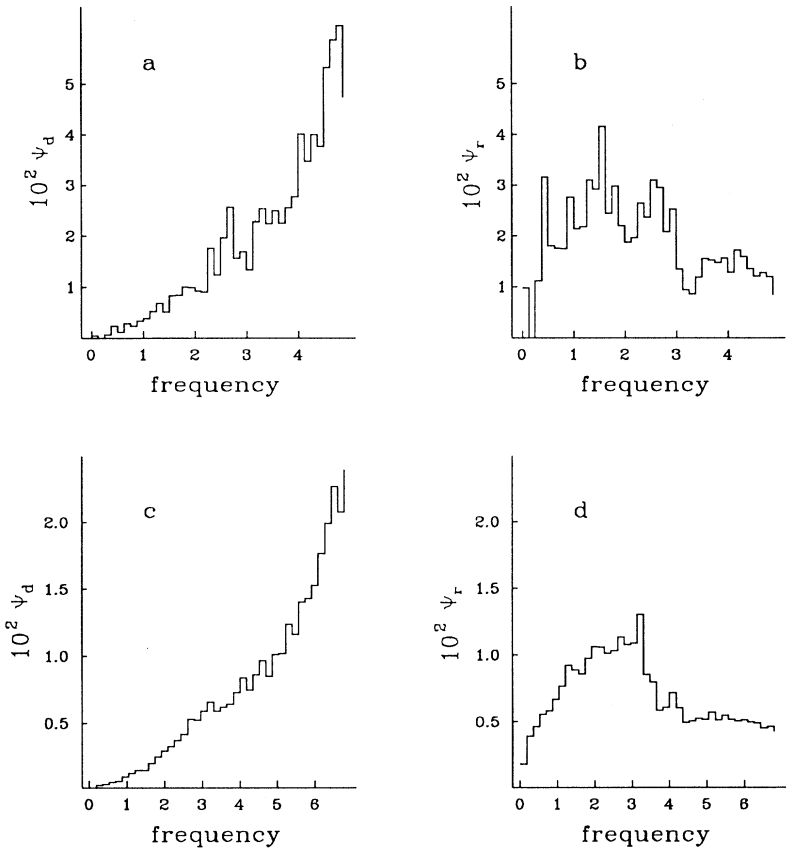

FIG. 10. The value of the divergence (a,c) and rotor (b,d) of the displacement field for clusters with $N = 80$ (a,b) and $N = 300$ (c,d) particles.

$$\langle u^2 \rangle = \frac{T}{N} \sum_{k=2}^{2N} \omega_k^{-2} \,, \tag{21}$$

from which we find the melting temperature T using the relation $\langle u^2 \rangle = \gamma l_0^2$, where $\gamma = 0.10$ for a 2D Wigner crystal,[21,22] and l_0 is the mean interparticle distance. As discussed in previous section, there exists a number of configurations with $\omega_{\min}$ very small, which will give a very large contribution to the sum (21). In order to see what the effect is of these very low frequency excitations on the melting temperature, we also considered the sum without the first term. Then we will find the temperature for intershell diffusion. Because for large clusters, the value of the interparticle distance around the center and near the periphery can be considerably different, therefore we will use the mean value of relative displacement in order to define the melting temperature,

$$T = \gamma N \left[\sum_{i=1}^{N} l_i^{-2} \sum_{k=2}^{2N} \vec{A}_i^2(k)/\omega_k^2 \right]^{-1} \,, \tag{22}$$

where $\vec{A}_i(k)$ is the displacement vector for the i particle in mode k, and l_i is the mean interparticle distance for the ith particle.

The numerical results are shown in Fig. 11. As we expect there is a significant difference in the transition temperature whether intershell rotation is taken into account or not. These results agree qualitatively with the results of Ref. 14, where it was found that (i) for clusters with a small number of particles the angular order is destroyed at much lower temperatures than the radial order, which agrees with the large difference in melting temperatures shown in Fig. 11; (ii) for larger clusters both temperatures are practically equal as is also apparent in Fig. 11. Orientational order and radial order disappear practically at the same temperature for $N > 40$; and (iii) the melting temperature at which intershell diffusion sets in, is a decreasing function of the number of particles in the cluster up to about $N \sim 20$–40, beyond which it starts to increase, which agrees qualitatively with Fig. 11. The magnitude of the transition temperature found in the present approach is slightly higher than found in the Monte Carlo study of Ref. 14. This is a consequence of the present harmonic approximation, which has a limited validity near the melting temperature. The melting temperature for intershell rotation (top part of Fig. 11) is strongly influenced by the value of $\omega_{\min}$, which is proportional to the rigidity of the cluster agains intershell rotations. In fact, it is a measure of the stability of the cluster against intershell rotations. As was mentioned before the value of $\omega_{\min}$, and also U_*, is determined by the configuration of the cluster. Clusters with a magic number of particles have a large melting temperature for intershell rotation. These fine details were not present in Ref. 14.

It is known that for an infinite crystal, the sum (22) diverges logarithmically in the low-wavelength, which is due to the presence of lateral sound waves. Therefore, one uses the average square displacement of interparticle distance in Lindeman's melting criterion. In our case, such criterion gives the relation

$$T = \gamma N \left[\sum_{i=1}^{N} l_i^{-2} \sum_{k=2}^{2N} \omega_k^{-2} \frac{1}{M} \sum_{m=1}^{M} \left[\vec{A}_i(k) - \vec{A}_m(k) \right]^2 \right]^{-1}, \tag{23}$$

where the sum over m runs over the M neighbor particles. The numerical results obtained using Eq. (23) is shown in Fig. 12. These results are very close to those found in Ref. 14 with the exception that here near $N \sim 150$ a maximum is found while the Monte Carlo results slowly increases towards the $N \to \infty$ value. We want to emphasize that if the number of particles is not too large, the transition temperature obtained with the second criterion (23) is lower than the one from Eq. (22). This indicates that the particles mainly move towards each other, and only for $N \geq 200$, the effect of small wave vectors begin to appear. In the latter case the neighbor particles move with the same velocity and the difference in the value of critical temperatures obtained using the spectrum of the eigenvibrations (Fig. 11) and the Monte Carlo technique[14] is very small.

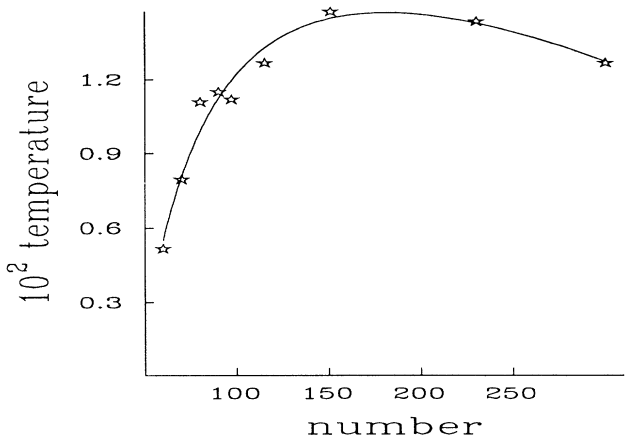

FIG. 12. Melting temperature for large clusters as obtained from Lindeman's melting criterion, excluding intershell rotation, and incorporating the relative displacement of neighbor particles.

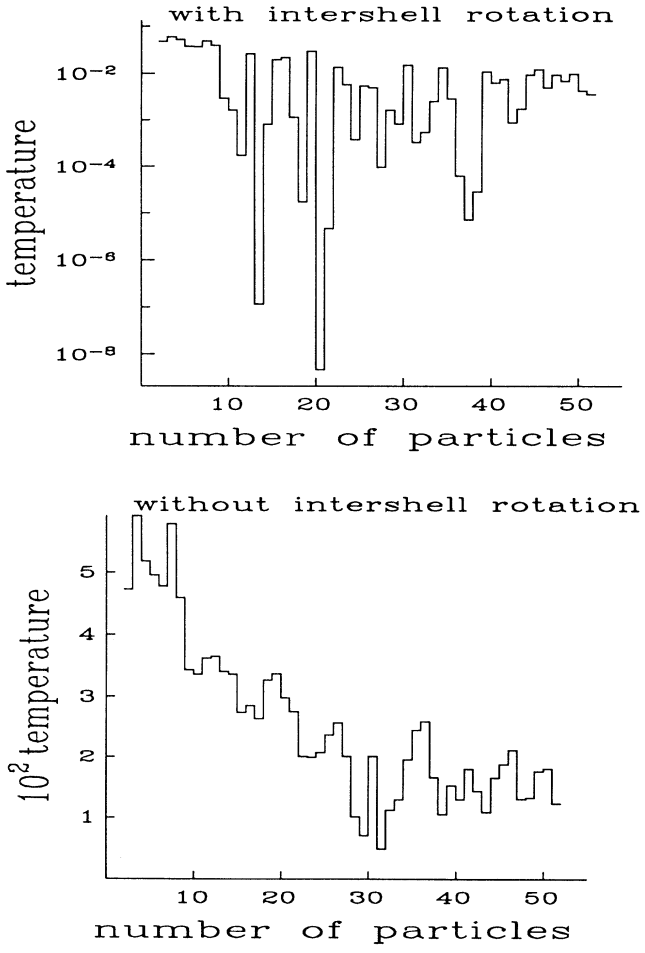

FIG. 11. Temperature of cluster melting obtained using the Lindeman criterion with and without intershell rotation.

VIII. SPECIFIC HEAT

Before we already mentioned that, in order to obtain the ground state, we generated many initial configurations and in so doing not only stable states but also metastable states were obtained. Thus, if we also calculate the spectrum of normal modes ω_k for each local minimum, we can easily obtain the partition function within the harmonic approximation and, consequently, all the thermodynamic quantities like the free energy, the specific heat,.... Such an approach was followed in Refs. 23 and 24 for 3D clusters, where the influence of anharmonicity and saddle points on the partition function was also studied. In Refs. 23, 24 only, the main characteristics of the spectrum of normal modes was used. Here we know the complete spectrum of our finite 2D system and are, therefore, able to calculate the partition function more correctly.

In the quasiclassical approximation, the partition function for a cluster with N particles is given by[25]

$$Z(T) = (2\pi\hbar)^{-2N} \int d\vec{q} d\vec{p} \exp\left[-H(\vec{q},\vec{p})/k_B T\right], \tag{24}$$

where $\vec{q} = (\vec{r}_1, ..., \vec{r}_N)$, $\vec{p} = (\vec{p}_1, ..., \vec{p}_N)$ are $2N$-dimensional vectors. The partition function can be written as

$$Z(T) = \sum_{m=1}^{M} \exp\left(-U_m/T\right) Z_m(T), \tag{25}$$

where Z_m is the partition function of the mth metastable

TABLE II. Shell configuration $(N_1, N_2, \ldots)$ for some metastable states for a number of different clusters. U_m is the energy difference of the metastable configuration with the ground-state energy and $W_m = \prod \omega_{k,m=1} / \prod \omega_{k,m}$ is the relative statistical weight.

N	$N_1, N_2, \ldots$	U_m	W_m
9	1,8	5.526×10^{-2}	3.14
25	3,8,14	5.308×10^{-2}	0.81
	4,8,13	1.013×10^{-1}	22.70
34	1,6,11,16	9.114×10^{-3}	15.91
	1,7,11,15	1.003×10^{-2}	79.70
	1,5,11,17	1.581×10^{-2}	7.22
	6,12,16	1.847×10^{-2}	60.60

state whose energy differs with the ground state by an amount U_m. The dimensionless units for temperature and specific heat are used here and below. In the vicinity of this mth metastable state, the Hamiltonian is quadratic in the normal coordinates. Because the energy barrier for intershell rotation is small, the effect of anharmonicity will already appear at low temperatures. Therefore, we will integrate only over a small region of particle motion $| q_i | \leq \sqrt{2U_m(k)/T\omega_{k,m}}$, which results in

$$Z_m = g_m Z_{\rm rot} \prod_{k=2}^{2N} \frac{T}{\hbar\omega_{k,m}} \mathrm{erf}(\sqrt{U_m(k)/T}), \qquad (26)$$

where $Z_{\rm rot} \propto \sqrt{T}$ is the part of the partition function resulting from the rotational degrees of freedom, $g_m = 2\pi/\theta_*$ is the degeneracy of the mth state, which is determined by the number of particles occupying a shell, $U_m(k)$ is the barrier height for normal mode k, and $\mathrm{erf}(x)$ is the error function. These parameters are given in Table II for a number of metastable states.

For convenience let us consider only one normal mode. At low temperature $T \ll U_m(k)$, expression (26) results in the usual value for the specific heat for a harmonic oscillator $C = 1$. For high temperature $T \ll U_m(k)$, the specific heat equals 1/2 as for free motion. For the intermediate temperature region $T \sim U_m(k)$, expression (26) gives an interpolation between these two limiting cases. Unfortunately, we know only the value of the barrier height for intershell rotation. For the remaining normal modes, we will use the analogy with the Lindeman criterion to write the phenomenological relation,

$$U_m(k) = \gamma_u N \frac{\omega_{k,m}^2 l_0^2}{2} , \qquad (27)$$

where l_0 is the mean interparticle distance, and $\gamma_u = 0.2$–0.3. The above expression is then used in the numerical evaluation of the partition function (26) and (25). Below we will mainly deal with the specific heat,

$$C = \frac{\partial}{\partial T} T^2 \frac{\partial \ln Z}{\partial T} , \qquad (28)$$

which is shown by the solid curve in Fig. 13.

General features of the behavior of the specific heat as a function of T and N can be predicted without detailed information regarding the metastable states and the spectrum of the normal modes. At low temperatures such that $T \ll (U_m(k), U_m)$, the specific heat is only determined by the ground state, and the effect of anharmonicity is not essential. Consequently, $C = 2N - 1/2$, as is apparent in Fig. 13. Usually the barrier for inter-

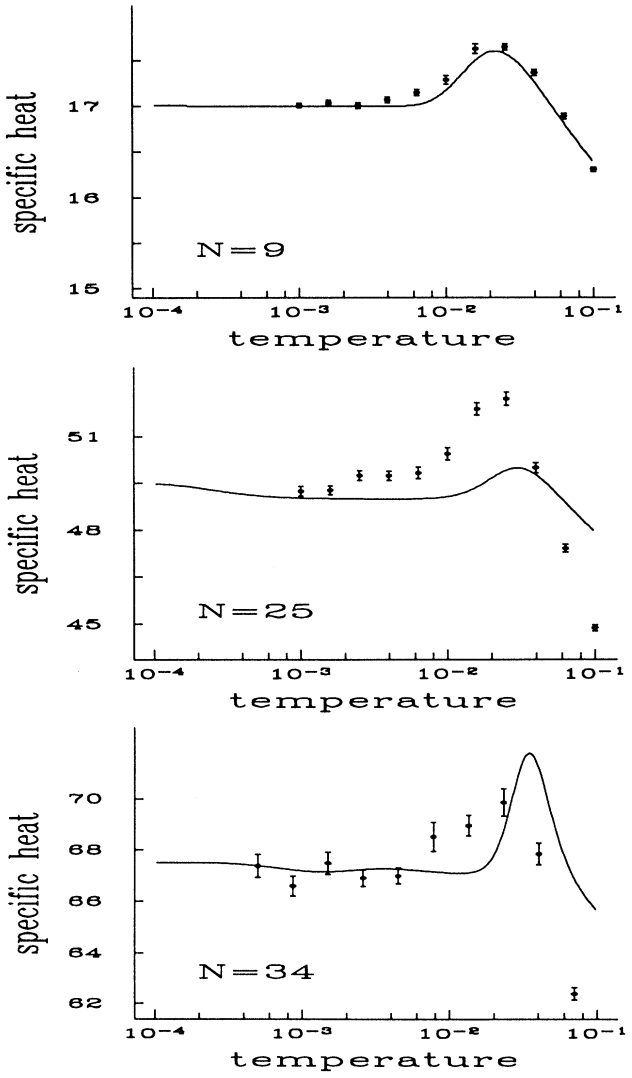

FIG. 13. Specific heat for clusters with $N = 9$, 25, and 34 particles, as a function of temperature. Solid lines are the results as obtained from an approximate calculation of the partition function, and the solid dots are results from the Monte Carlo simulation.

shell rotation is the smallest energy, which is also smaller than the difference in energy between the ground state and the metastable states. In the temperature range $U_1(k=2) \ll T \ll (U_1(k \neq 2), U_m)$, the specific heat will be constant and having the value $C = 2N - 1$. Such a small reduction in C is visible in Fig. 13 near $T \sim 10^{-3}$. With further increase of the temperature, the behavior of the specific heat is determined by the competition of two processes. On the one hand, transitions to metastable states which lead to an increase of the specific heat, and on the other hand, the effect of anharmonicity which will reduce C. This interplay will lead to peaks in the specific heat as is apparent in Fig. 13. Note that the position of the peak does not equal the melting temperature.

In the order-disorder transition region the applicability of the above approach is questionable. Therefore, we also calculated the specific heat using the standard Monte Carlo technique. As the initial state, we took the ground state of our system. Then we fix the temperature and execute 10^5 steps of the Metropolis algorithm to allow the system to achieve equilibrium. Next about $(4\text{–}10) \times 10^6$ steps of the Metropolis algorithm are made in order to reduce the statistical error. The specific heat is then found using the following formula:

$$C = N + (\langle E^2 \rangle - \langle E \rangle^2)/T^2 \ , \tag{29}$$

where E is the potential energy for the system with N particles. In Fig. 13, we compare the results from the Monte Carlo simulation (full dots) with the above results (full curve), which are based on the excitation spectrum of the $T = 0$ stable and metastable states. Note that for the small cluster with $N = 9$ very good agreement is obtained. For the other two clusters, good quantitative agreement is found at low temperature while at intermediate and high temperatures only the qualitative behavior is correctly described. Thus, for large clusters the approximate model is not able to give a satisfactory description of the effect of anharmonicity. Nevertheless there is qualitative agreement in the position of the maxima. We have tried to vary the parameter γ_u and to change the integration interval for the allowed particle motion in Eq. (26), but we were not able to obtain any better agreement.

IX. CONCLUSION

We have presented the results of a numerical simulation of the ground state and the spectrum of normal modes of classical 2D clusters with quadratic confinement. The barriers for intershell rotation and the specific heat are also obtained. The Lindeman melting criterion in conjunction with the $T = 0$ excitation spectrum of the ground-state configuration was used to obtain the order-disorder transition temperatures for angular and radial melting.

For systems with axial symmetry, and an intermediate number of particles, the normal mode with the lowest frequency corresponds to intershell rotation if there are at least two shells. A low excitation energy for intershell rotation is found for clusters which have a shell configuration such that the number of particles on each shell have no common multiple. If the number of particles in the outer shell is an integer multiple of the number of particles in the inner shell, the cluster will be most stable against intershell rotation, which define the clusters with magic numbers. Such clusters also have a large melting temperature for intershell rotation. Distortion of the axial symmetry of the external potential, will lead to a rise in the eigenfrequency and in the barrier height for intershell rotation. For large clusters, i.e., $N > 100$, the normal mode with the lowest frequency corresponds to a vortex/anti-vortex excitation.

ACKNOWLEDGMENTS

We wish to thank our colleague V.M. Bedanov for fruitful discussions. Part of this work was supported by INTAS Grant No. 93-1495, the Human Capital and Mobility network Programme No. ERBCHRXT 930374, and the Belgian National Science Foundation.

* Permanent address: Institute of Theoretical and Applied Mechanics, Russian Academy of Sciences, Novosibirsk 630090, Russia.

† Author to whom correspondence should be addressed. Electronic address: peeters@uia.ua.ac.be

[1] P.E. Toschek, in *New Trends in Atomic Physics*, edited by G. Grynberg and R. Stora (North-Holland, Amsterdam, 1984), Vol. I, p. 383.

[2] B.G. Levi, Phys. Today **41**, 17 (1988); G. Birkl, S. Kassner, and H. Walther, Europhys. News **23**, 143 (1992).

[3] A. Rahman and J.P. Schiffer, in *Condensed Matter Theories,* edited by P. Vashishta, R.K. Kalia, and R.F. Bishop (Plenum, New York, 1987), Vol. 2, p. 33.

[4] J.H. Chu and Lin I, Phys. Rev. Lett. **72**, 4009 (1994); H. Thomas, G.E. Morfill, V. Demmel, J. Goree, B. Feuerbacher, and D. Möhlmann, *ibid.* **73**, 652 (1994).

[5] P. Leiderer, W. Ebner, and V.B. Shikin, Surf. Sci. **113**, 405 (1987).

[6] *Nanostructure Physics and Fabrication*, edited by M.A. Reed and W.P. Kirk (Academic, Boston, 1989).

[7] Y. Kondo, J.S. Korhonen, M. Krusius, V.V. Dmitriev, E.V. Thuneberg, and G.E. Volovik, Phys. Rev. Lett. **68**, 3331 (1992).

[8] D. Reefman and H.B. Brom, Physica **183C**, 212 (1991).

[9] G.E. Volovik and U. Parts, Pis'ma Zh. Eksp. Teor. Fiz. **58**, 826 (1993) [JETP Lett. **58**, 774 (1993)].

[10] R. Rafac, J.P. Schiffer, J.S. Hangst, D.H.E. Dubin, and D.J. Wales, Proc. Natl. Acad. Sci. U.S.A. **88**, 483 (1991).

[11] K. Tsuruta and S. Ichimaru, Phys. Rev. A **48**, 1339 (1993).
[12] Yu. E. Lozovik and L.M. Pomirchy, Phys. Status Solidi B **161**, K11 (1990); Yu. E. Lozovik and V.A. Mandelshtam, Phys. Lett. A **145**, 269 (1990); **165**, 469 (1992).
[13] F. Bolton and U. Rössler, Superlatt. Microstruct. **13**, 139 (1993).
[14] V.M. Bedanov and F.M. Peeters, Phys. Rev. B **49**, 2667 (1994).
[15] B. Tanatur and D.M. Ceperley, Phys. Rev. B **39**, 5005 (1989).
[16] K. Jauregui, W. Häusler, and B. Kramer, Europhys. Lett. **24**, 581 (1993).
[17] N. Metropolis, A.W. Rosenbluth, M.N. Rosenbluth, A.M. Teller, and E. Teller, J. Chem. Phys. **21**, 1087 (1953).
[18] L. Bonsall and A.A. Maradudin, Phys. Rev. B **15**, 1959 (1977).
[19] D.S. Fisher, B.I. Halperin, and R. Morf, Phys. Rev. B **20**, 4692 (1979).
[20] F. Lindeman, Z. Phys. **11**, 609 (1910).
[21] Yu.E. Lozovik and V.M. Fartzdinov, Solid State Commun. **54**, 725 (1985).
[22] V.M. Bedanov, G.V. Gadiyak, and Yu.E. Lozovik, Phys. Lett. **109A**, 289 (1985).
[23] M. Bixon and J. Jortner, J. Chem. Phys. **91**, 1631 (1989).
[24] S.F. Chekmarev and I.N. Umirzakov, Z. Phys. D **26**, 373 (1993).
[25] *Statistical Physics*, edited by L.D. Landau and E.M. Lifshitz (Pergamon Press, New York, 1980), p. 91.